DOI: 10.1002/cssc.201301262

Construction of High-Energy-Density Supercapacitors from Pine-Cone-Derived High-Surface-Area Carbons

Kaliyappan Karthikeyan,*[a, b] Samuthirapandiyan Amaresh,[a] Sol Nip Lee,[a] Xueliang Sun,[b] Vanchiappan Aravindan,[c] Young-Gi Lee,[d] and Yun Sung Lee*[a]

Very high surface area activated carbons (AC) are synthesized from pine cone petals by a chemical activation process and subsequently evaluated as an electrode material for supercapacitor applications in a nonaqueous medium. The maximum specific surface area of ~3950 $m^2 g^{-1}$ is noted for the material treated with a 1:5 ratio of KOH to pine cone petals (PCC5), which is much higher than that reported for carbonaceous materials derived from various other biomass precursors. A symmetric supercapacitor is fabricated with PCC5 electrodes, and the results showed enhanced supercapacitive behavior with the highest energy density of ~61 Wh kg^{-1}. Furthermore, outstanding cycling ability is evidenced for such a configuration, and ~90% of the initial specific capacitance after 20000 cycles under harsh conditions was observed. This result revealed that the pine-cone-derived high-surface-area AC can be used effectively as a promising electrode material to construct high-energy-density supercapacitors.

Introduction

The search for new alternative electrochemical energy-storage devices for hybrid electric vehicle (HEV) and electric vehicle (EV) applications have been accelerated because of the depletion of oil resources/hike in oil prices and an increasing awareness of environmental concerns.[1] Among the electrochemical energy-storage systems, electrochemical double-layer capacitors (EDLCs) are expected to play a major role because of their high power capabilities with long life spans. One of the hot topics of research is to increase the energy density of such EDLCs.[2,3] In principle, electrical energy stored in an EDLC is based on the separation and pure electrostatic attraction of the charge carriers across the electrode and ionically conductive electrolyte interface (non-Faradaic mechanism). Such a non-Faradaic reaction occurs predominantly on the surface of the carbonaceous electrodes irrespective of the use of an aqueous or organic medium.[2] So far, a variety of carbonaceous materials has been investigated extensively for EDLC applications.[4–6] Among them, highly porous activated carbons (ACs) with unique characteristics such as a high specific surface area, high electrical conductivity, chemical and thermal stability, and relatively low cost are promising electrode materials for such applications.[4,6,7]

The choice of raw material and the associated activation process (either chemical or physical activation) are the most important factors that influence the electrochemical profiles of AC.[2,6] Conventional ACs derived from, for example, coal, petroleum coke (PC), needle coke (NC), and biomass precursors, exhibit different electrochemical performances, which indicates the importance of the precursor.[7–10] Although ACs obtained from traditional precursors such as cokes and coal exhibit a high specific surface area $>2000\ m^2 g^{-1}$ and good capacitance properties, difficulty in the activation of cokes and the associated environmental pollution is the main issue.[7,10] Therefore, a lot of research activity is focused on the development of biomass-derived AC with excellent textural properties.[10,11] So far, few reports describe the use of biomass-derived ACs for supercapacitor applications with either aqueous, organic, or ionic liquid electrolytes, for instance, coconut shell,[12–14] eucalyptus wood,[12] fir wood,[15,16] bamboo,[17] banana fiber,[18] corn grains,[19] sugar cane bagasse,[20] apricot shell,[21] sunflower seed shell,[22] potato starch,[12] coffee ground,[23,24] wheat straw,[25] fish scale,[26] chicken egg-shell membrane,[27] cherry stone,[28] rice husk,[29] recycled waste paper,[30] cassava peel waste,[31] pistachio shell,[16] argan seed shell,[32] seaweeds,[33] and dead neem leaves.[11] Generally, ACs derived from these sources exhibit a specific surface area between 1000–3000 $m^2 g^{-1}$ and show good specific capacitance properties.[10] Haykırı-Açma[34] first studied the synthesis of

[a] Dr. K. Karthikeyan, S. Amaresh, S. N. Lee, Prof. Y. S. Lee
Faculty of Applied Chemical Engineering
Chonnam National University
Gwang-ju 500-757 (Republic of Korea)
E-mail: leeys@chonnam.ac.kr
kkaliyap@uwo.ca

[b] Dr. K. Karthikeyan, Prof. X. Sun
Department of Mechanical and Materials Engineering
The University of Western Ontario
London, Ontario, N6A 5B9 (Canada)

[c] Dr. V. Aravindan
Energy Research Institute (ERI@N)
Nanyang Technological University
Research Techno Plaza, 50 Nanyang Drive, Singapore 637553 (Singapore)

[d] Dr. Y.-G. Lee
Power Control Device Research Team
Electronics and Telecommunications Research Institute
Daejeon 305-700 (Republic of Korea)

Supporting information for this article is available on the WWW under http://dx.doi.org/10.1002/cssc.201301262.

pine-cone-derived carbonaceous materials with a high yield (>40%) and minimum ash content (0.7 wt%). This minimum ash content and notable carbon yield makes pine cones attractive for the synthesis of high-surface-area AC for manifold applications compared to other biomass precursors reported.[34,35] Furthermore, pine cones or coulter pines and their seeds are a common form of biomass, which is highly abundant, low cost, and has existed for over 200 million years. Pine cones are used predominantly for decorative applications, food preparation, and baking. Nevertheless, reports have described the synthesis of pine-cone-derived AC for the removal of Pb ions from water[36] and their adsorption properties for various dyes.[37–39] Recently, Duman et al.[35] evaluated the physical and chemical properties of such a pine-cone-derived AC and confirmed the low ash content and high yield. The abovementioned appealing properties of pine-cone-derived AC attracted us to evaluate its supercapacitance behavior in an EDLC configuration with the need to enhance the energy density in mind. To realize the higher energy density of EDLCs, the use of organic electrolytes is necessary as aqueous electrolytes experience oxygen evolution at ~1.23 V.[6,40] In this regard, high-surface-area AC was prepared by activation of the charcoal obtained from the carbonization of pine cones with KOH at two different concentrations. Among the samples prepared, the AC treated with a high concentration of activation agent (KOH) had an ultrahigh surface area of ~3950 $m^2 g^{-1}$ along with enhanced structural alignment and high electrical conductivity. The high-surface-area AC obtained was tested as an electrode material in an EDLC configuration in an organic medium. The EDLC cell that contained the AC with 5 wt% KOH delivered a high capacitance of 198 $F g^{-1}$ and an energy density of 61 $Wh kg^{-1}$ between 0 and 3 V at 0.25 $A g^{-1}$ current density. Various studies were conducted to corroborate the results that were obtained and are described in detail.

Results and Discussion

The XRD pattern of raw pine cone petals (RPP) is presented in Figure S1a. The XRD pattern of RPP exhibits the main characteristic peaks of cellulose I at $2\theta =$ 15.9, 22.1, and 34.3° and less organized peaks that correspond to cellulose II at $2\theta =$ ~26, ~36, and ~40°, which indicates that RPP is composed mainly of highly organized crystalline cellulose fibers.[41–43] The surface morphology (Figure S1b) shows clearly that RPP is composed of large microfibers with an external diameter of ~45 μm. Moreover, the presence of macropores between the fibers (Figure S1c) was also noted. The surface composition of RPP was examined by FTIR spectroscopy (Figure S1c), which suggests that RPP is composed of a mixture of functional groups. The peaks observed at $\tilde{\nu} = 1610$ and 690 cm^{-1} are related to the existence of lignin.[42] The stretching vibration of polysaccharide components such as the carbohydrate backbone (C–C), symmetric glycosidic groups (C–O–C), the cellulose backbone (C–OH), and the O–H and C–H groups of cellulose are observed at $\tilde{\nu} = 1160$, 1100, 1050, ~1330, and 2910 cm^{-1}, respectively.[43] The stretching vibration of C=O in the protonated carboxylic acid because of the presence of uronic acids was confirmed by the peak at $\tilde{\nu} =$ ~1720 cm^{-1}.[42,43] Notably, the texture of the raw material (RPP in this case) influences the surface area of the carbon. The existence of a large quantity of macropores on RPP is conducive to absorb more activation agent (KOH), which enables the complete oxidation of the reactive sites to form a more porous surface (Figure S1c). Hence, a very high surface area can be achieved with a high amount of activation agent.[10]

The XRD patterns of PCC0, PCC3, and PCC5 pyrolyzed at 750 °C under an Ar flow are presented in Figure 1a. The obtained patterns suggest clearly the highly disordered/amorphous nature of the carbons derived from pine cones with discernible characteristic (002) and (001) reflections. The broad reflections between $2\theta = 20$ and 30° (002) indicate the presence of small domains of coherent graphene sheets, whereas the reflections around $2\theta = 43°$ (001) correspond to the 3D honeycomb structure formed by the sp^2-hybridized carbon

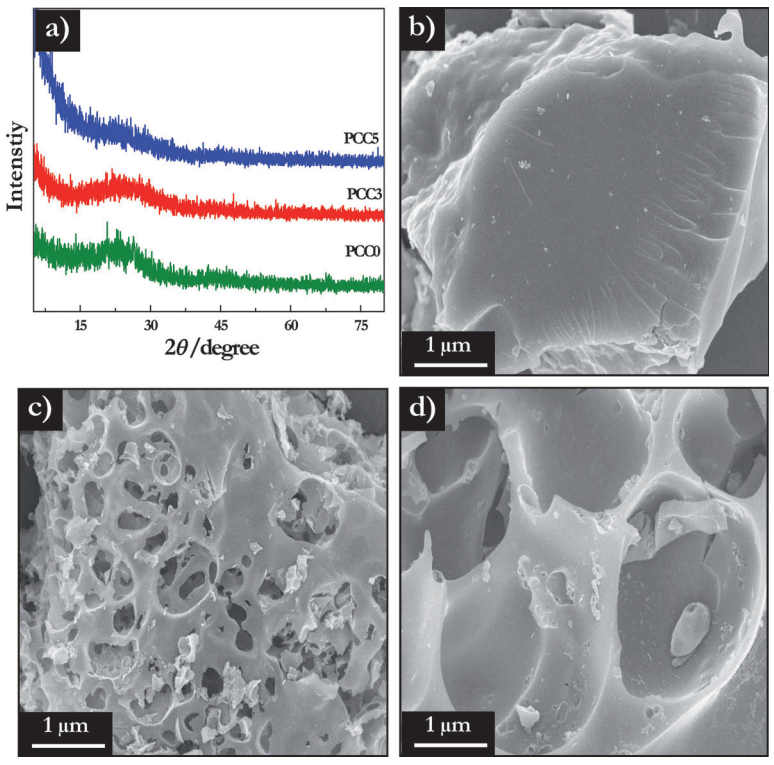

Figure 1. a) XRD patterns of PCC0, PCC3, and PCC5 prepared at 750 °C and field-emission scanning electron micrographs of b) PCC0, c) PCC3, and d) PCC5.

atoms.[17] Although no discernible peaks are observed, a decrease in the peak intensity is noted as the KOH loading is increased during activation. This reveals the increase in *d* spacing, which leads to ACs with a disordered nature to result in a larger specific surface area. It is well known that the measurement of the empirical parameter (*R* factor) is an effective way to evaluate the number of graphene sheets arranged as a single layer. This *R* factor can be defined as the ratio of the intensity of the (002) reflection with respect to the background.[44,45] The more prominent (002) reflection for PCC0 than that of the KOH-treated samples indicates a higher degree of carbonization. As expected (Table 1), a decrease in the *R* factor on increasing the KOH ratio suggests that the activation process leads to a breakdown of aligned structural domains, that is, long-range order and allows the random distribution of graphene nanosheets.[45] However, the sample with a lower empirical value exhibits a large number of single layers, which results in better textural characteristics. Therefore, better capacitive properties are expected for PCC5 than the other materials prepared. The morphological features of pyrolyzed carbon from pine cones under an Ar flow are shown in Figure 1b–d. As expected, there is no porosity generated in the case of pyrolyzed carbon, that is, if the PCC/KOH ratio is 1:0. Many open cavities are noted in PCC treated with the minimum amount of KOH (1:3 ratio), whereas a 3D architecture and interconnected network-like morphology are observed for the material prepared with a 1:5 ratio. The formation mechanism of the cavities on the surface was attributed to the intercalation of K^+ ions into the lamellae of the crystallites, which broke the lamellae arrangement to result in the expansion of the interlayer voids, elimination of crosslinking, and the stabilization of carbon atoms in the crystallites.[20,31] Although the K^+ ions were removed by washing with HCl, the reorganization of lamellae is not possible. Thus, it provides free interlayer voids, which is considered to be the key factor to achieve a very high surface area. Such a morphology is beneficial for facile electron transport and to enable more active sites for the double-layer formation across the interface, which results in more favorable electrochemical characteristics irrespective of a symmetric or asymmetric assembly.[6,7]

Table 1. Textural parameters of PCC samples obtained from N_2 adsorption–desorption isotherms.

Sample	*R* factor	BET surface area [$m^2 g^{-1}$]	Pore volume [$cm^{-3} g^{-1}$]	Pore diameter [nm]	S_{micro} [$m^2 g^{-1}$]	Micropore volume [$cm^3 g^{-1}$]
PCC0	2.27	569	0.250	1.7	728	0.19
PCC3	1.94	2140	1.214	2.1	1993	0.57
PCC5	1.71	3950	2.395	2.9	3645	1.72

The nitrogen adsorption–desorption isotherms of AC derived from pine cones are presented in Figure 2a. Notably, shape of the isotherms varied remarkably with KOH treatment. The isotherm of PCC0 indicates type I behavior according to the IUPAC classification. In contrast, the curves of PCC3 and PCC5 exhibit an intermediate isotherm between type I and II with a knee and increasing plateau, which suggests a combination of micro- and mesoporous structures in the samples. The early stage of the isotherms corresponds to micropore filling, and the sloppy region at a high relative pressure represents the multilayer adsorption on the mesopores. In addition, if the amount of activation agent is increased, the nitrogen adsorption properties of the AC also increased with relative pressure until $P/P_0 \approx 0.5$. It is well known that an isotherm with a slight hysteresis loop and wide knees

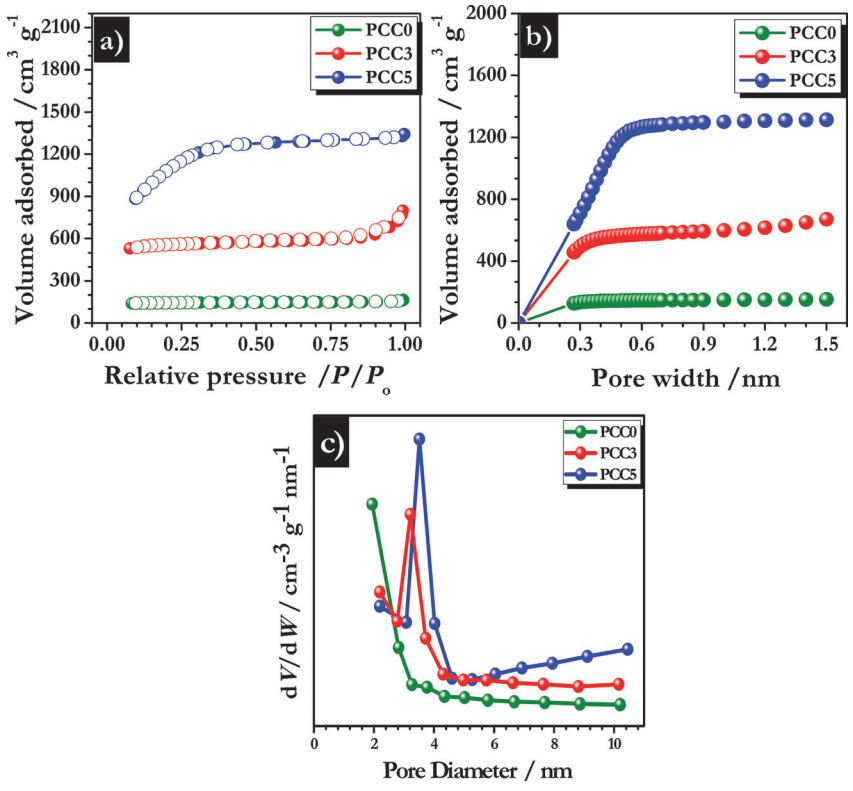

Figure 2. a) Nitrogen adsorption–desorption isotherms, b) pore width versus volume adsorption, and c) pore size distribution of the prepared carbon samples.

at P/P_0 of around 0.35–0.5 indicates the presence of a considerable amount of small mesopores, which can be observed on the PCC5 surface. The porous textural parameters of ACs derived from pine cones, such as BET surface area, micropore volume, and the average pore diameter, are summarized in Table 1. It is evident that the BET surface area and total pore volume of the samples increase remarkably after the introduction of the KOH activation agent. Among the samples, PCC5 shows the highest surface area (3950 $m^2 g^{-1}$) and pore volume, which demonstrate the well-developed porous structure. However, PCC0 exhibited poor textural properties with a surface area and pore volume of 569 $m^2 g^{-1}$ and 0.25 $cm^3 g^{-1}$, respectively. Notably, the BET surface area obtained for PCC5 is comparable to the highest value ever reported for AC obtained from a biomass precursor.[10,11] PCC5 showed a larger absorption volume than PCC0 and PCC3 (Figure 2b), which indicates a higher surface area and larger pore volume with a favorable pore size distribution. The pore size distributions of all the samples measured by N_2 adsorption are illustrated in Figure 2C. These indicate that the addition of KOH significantly affects the pore size distribution, and an increased KOH weight ratio can enlarge the pore size (Figure 2c). Both PCC3 and PCC5 have a pore size around 3–4 nm, whereas the pore size of PCC0 is less than 2 nm. Moreover, PCC3 and PCC5 also showed microporosity. This could be because pine cone petals localize the carbon rods inside the structures during carbonization. Furthermore, with the increased KOH concentration, more KOH is believed to take part in the activation process to result in a more porous structure, which leads to an increase in the surface area of the samples. Moreover, the addition of a larger amount of activation agent (KOH) provides extra surface oxygen complexes that release more carbonaceous gases and allow a slower and controlled carbonization reaction, which is responsible for the enhancement of the porosity as well as the surface area of the resultant material. The ultrahigh surface area and narrow pore size distribution of PCC5 is beneficial for charge-storage applications.[40]

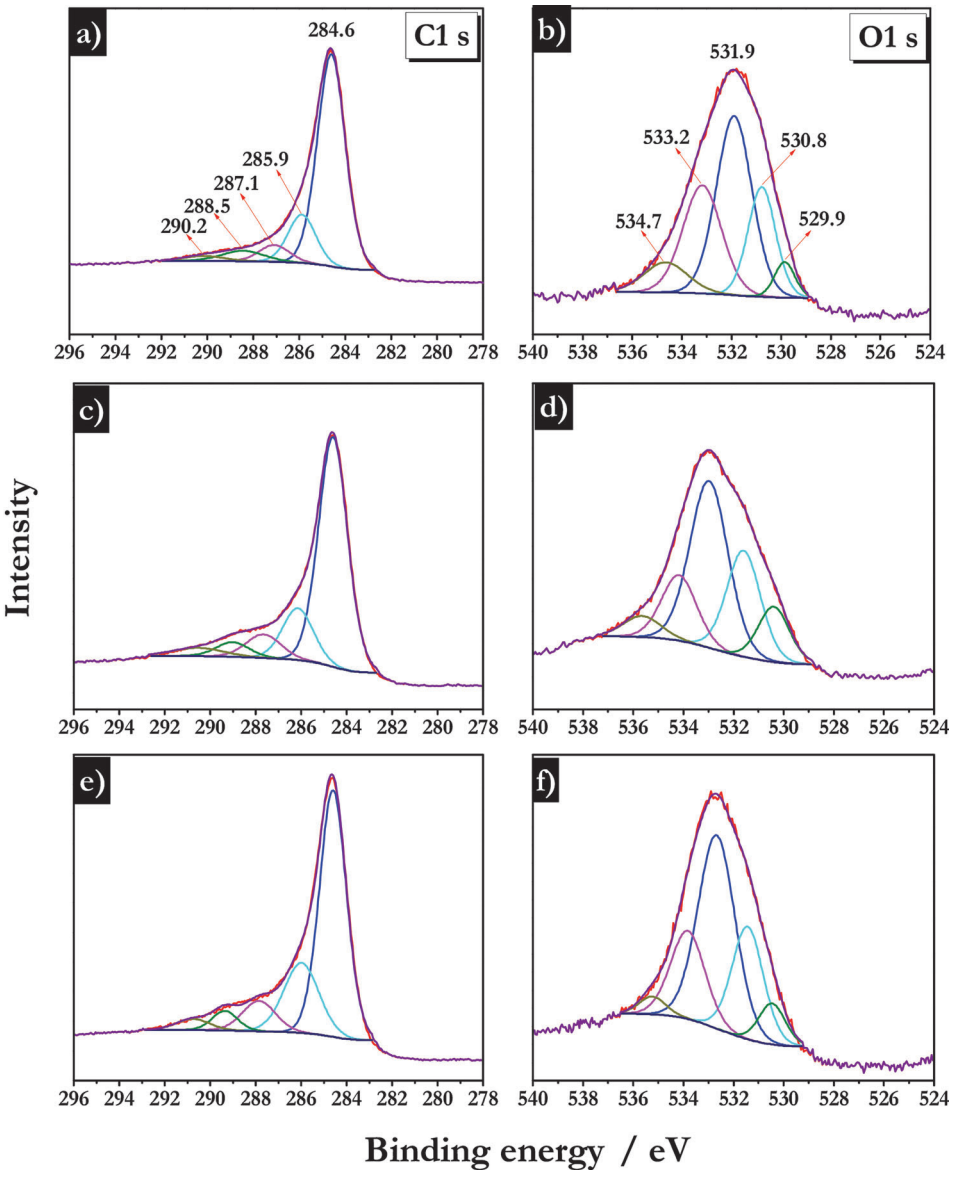

Figure 3. Core-level (C 1s and O 1s) XPS spectra of a, b) PCC0, c, d) PCC3, and e, f) PCC5.

The surface features of the pine-cone-derived ACs were analyzed by X-ray photoelectron spectroscopy (XPS; Figure 3). The core-level C 1s and O 1s spectra show the presence of functional groups over the AC surface clearly. In the core-level C 1s spectra, the sp^2 C–C binding energy is centered around 284.6 eV, and the appearance of peaks at binding energies of 287.1 and 288.5 eV correspond to carbonyl (C=O) and carboxyl (O=C–OH) groups, respectively. The peaks positioned around 285.9 and 290.2 eV are assigned to the hydroxyl groups (C–OH) and π–π^*, respectively.[46,47] An increased intensity of all the peaks is noted with increased KOH concentration, which suggests clearly that the activating agent plays a vital role to develop these active functional groups.[46–48] Similarly, in the core-level O 1s spectra, the appearance of peaks at binding energies of 534.7, 533.2, 530.8, and 529.9 eV also reflects the presence of the functional groups noted above.[47] Furthermore, oxygen contents of ~12.66, ~19.02, and ~14.41 wt%

(atomic) are calculated for PCC/KOH ratios of 1:5, 1:3, and 1:0, respectively. According to Simon and Gogotsi,[40] the presence of a small amount of oxygen-containing functional groups is crucial to ensure the long-term cycleability of the carbonaceous materials. The presence of higher surface functionalities such as surface oxygen affects the electrical conductivity profile and is involved in an unwanted side reaction with the electrolyte counterpart. As a result, poor electrochemical profiles are noted for such oxygen-rich carbonaceous electrodes.[40] Therefore, a good electrochemical profile is noted for PCC5.

The Raman spectra of RPP, PCC0, PCC3, and PCC5 are illustrated in Figure S2. RPP did not show any peaks within the recorded area, whereas all other samples showed characteristic carbon peaks centered at $\tilde{\nu} = \sim 1350$ and 1595 cm^{-1}, which indicate the successful carbonization of the pine cone petals.[49] The peaks at $\tilde{\nu} = 1350$ and 1595 cm^{-1} could be assigned to disordered carbon (D band) and the symmetric E_{2g} vibration mode of graphite-like materials (G band), respectively.[49] In addition, the intensity ratio of the D and G bands (I_D/I_G) for PCC0, PCC3, and PCC5 was 1.17, 0.94, and 0.99, respectively. It is clear that the sample prepared with the highest KOH ratio showed a high structural alignment, which suggests that PCC5 contains predominantly sp^2-type carbon. However, the high structural alignment of PCC5 could effectively decrease the presence of heteroatoms (O, S, and N) on the surface, which would reduce the risk of side reactions and thus affect the charge-storage behavior. This correlates well with the result obtained from XPS analysis. In addition, the high structural alignment further confirmed the high degree of intralayer condensation of PCC5, which improved its electrical conductivity remarkably and enhanced the ionic/electronic transfer to lead to an excellent improvement in the electrochemical performance of the PCC5 electrodes.

The cyclic voltammetry (CV) traces of the symmetric supercapacitors fabricated with pine-cone-derived AC cycled between 0–3 V at scan rate of 50 mV s^{-1} are shown in Figure 4a. The CV curves revealed clearly the more or less rectangular behavior for all the three electrodes with variation in the current response that is characteristic of typical EDLCs.[2] At higher scan rates, the distortion of the CV signatures noted for all three electrodes suggests a diffusion-limited capacitance because of the polarization effect (Figure S3). From the CV studies, the energy-storage mechanism of such symmetric supercapacitors could be explained by electrical double-layer theory, which is mainly based on the accumulation of charge carriers across the electrode–electrolyte interface, which subsequently forms the double layer.[2,7] In this case, the symmetric cells delivered specific capacitances of ~141, ~100, and ~17 F g^{-1} at a slow scan rate of 5 mV s^{-1} for PCC5, PCC3, and PCC0, respectively. This increase in specific capacitance is consistent with the linear variation of the specific surface area of the ACs derived from pine cones and in the literature.[4] As expected, a decrease in the specific capacitance profiles are noted for all the three ACs with an increase in scan rate (Figure 4b).

Galvanostatic charge–discharge studies were performed for all the three symmetric supercapacitor cells between 0–3 V at a current density of 1 A g^{-1} (Figure 5a). The charge–discharge

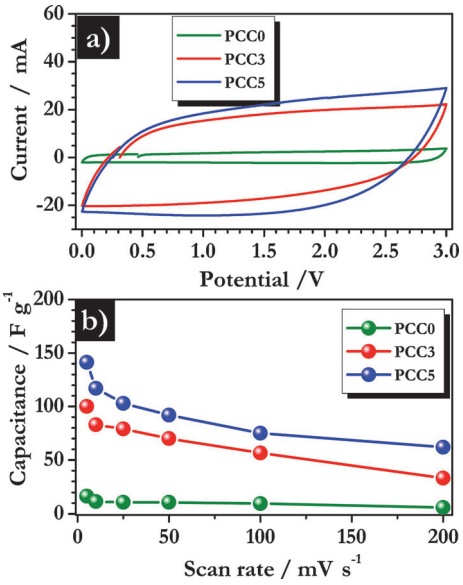

Figure 4. a) CV traces of PCC0, PCC3, and PCC5 electrodes in a symmetric supercapacitor configuration at a scan rate of 50 mV s^{-1} between 0 and 3 V and b) the dependence of capacitance versus scan rate.

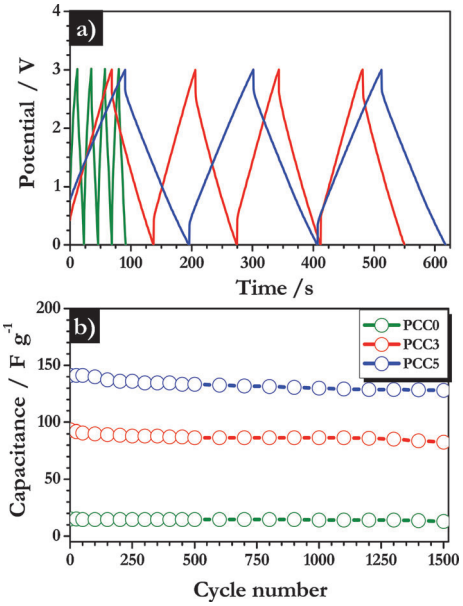

Figure 5. a) Typical charge–discharge of the symmetric supercapacitor cells at a current density of 1 A g^{-1}, and b) plot of specific discharge capacitance versus cycle number.

curves of all the cells show a linear relationship with time, which is indicative of perfect EDLC behavior. However, a sharp decrease in voltage is noted at the beginning of the discharge–charge that results from the equivalent series resistance (ESR) of the cell. The ESRs of symmetrical cells that contained PCC0, PCC3, and PCC5 electrodes were calculated as 50, 39, and 29 Ω, respectively. A longer charge–discharge time is noted for PCC5 compared to PCC3 and PCC0, which is consistent with the CV analysis.[4] The symmetric cells delivered a spe-

cific capacitance of ~142, ~92, and ~15 F g^{-1} at a current density of 1 A g^{-1} for the PCC5, PCC3, and PCC0 configurations, respectively. Accordingly, such cells retained ~92, ~89, and ~86% of the initial capacitance value after 1500 cycles (Figure 5b). Such enhanced supercapacitance behavior of pine-cone-derived AC is mainly because of the microporous nature of the carbonaceous materials. This is one of the prerequisites for the easy access of the electrolyte solution and thereby enables facile adsorption/desorption of PF_6^- anions especially at high current rates.[50] The enhancement in the specific capacitance performance is consistent with previous reports because of the existence of small pores with a high surface area, which provide a much higher capacitance than mesoporous materials according to Simon and co-workers[2,51] and Jain et al.[52] However, the porous texture, low ESR, high specific surface area, and micropore volume cannot be ruled out as reasons for such performance (Table 1).[2] Interestingly, the specific capacitance obtained for PCC5 symmetrical cells in organic solutions is one of the best results for carbon-based EDLCs in organic/ionic liquid media.[2,6,7,11,40]

The dependence of the specific capacitance on the current density is shown in Figure 6a. As expected, the discharge capacitance decreases linearly with an increasing current rate,

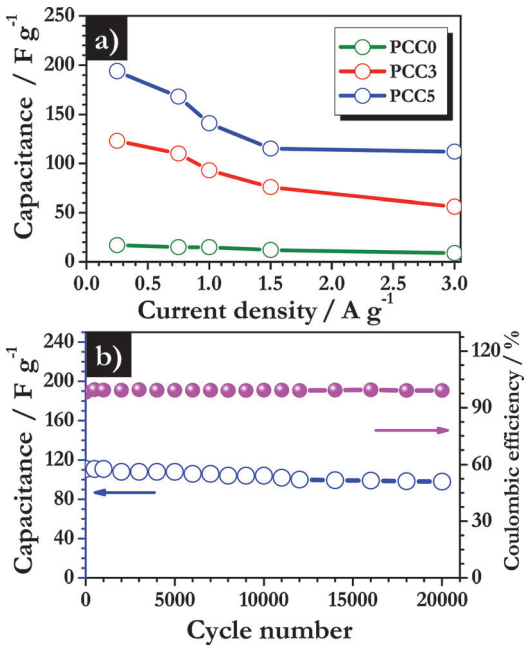

Figure 6. a) Rate performance of symmetric supercapacitor cells at various current densities and b) long-term cycling profiles of PCC5-based symmetric supercapacitor cells at 3 A g^{-1}.

which is consistent with CV studies. The PCC5-based symmetric cell delivered an excellent specific discharge capacitance irrespective of the applied current density, for example, ~198 and ~111 F g^{-1} were obtained at current densities of 0.25 and 3 A g^{-1}, respectively. Prolonged cycleability is a prerequisite for such EDLCs, therefore, long-term cycling studies were conducted for the best-performing configuration (i.e., PCC5) at a current density of 3 A g^{-1} (Figure 5b). In general, the cycleability of carbonaceous materials in organic solutes is inferior because of poor textural properties and poor ionic conductivity.[6] In the present case, exceptional cycleability is noted for the PCC5-based symmetric supercapacitor assembly, which retained ~90% of the initial capacitance (~111 F g^{-1}) after 20000 cycles with a Coulombic efficiency of over ~99.9%. This demonstrates clearly the remarkable reversibility of the pine-cone-derived AC (PCC5) in an organic medium. The outstanding capacitive performance of the PCC5 symmetrical cell is derived from its enhanced electrical conductivity and the presence of a higher percentage of mesopores.

To investigate the conductive nature of the synthesized AC, electrical impedance spectroscopy (EIS) was performed under open-circuit voltage conditions between 100 kHz and 100 mHz with an applied a.c. amplitude of 10 mV in the symmetric cell configuration. From the Nyquist plot (Figure 7), it can be seen

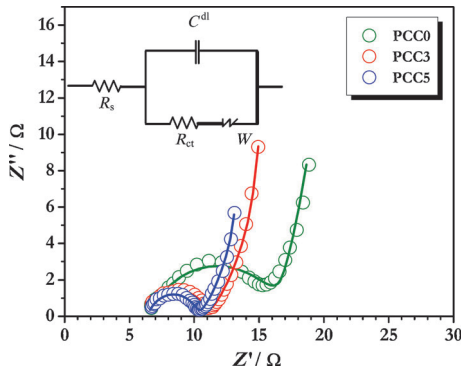

Figure 7. Nyquist plots of PCC0-, PCC3-, and PCC5-based symmetric supercapacitor cells under open-circuit voltage conditions between 100 kHz and 100 mHz.

that all the curves exhibited two main regions: a depressed semicircle in the high-frequency region, which is related to the charge-transfer resistance (R_{ct}), and a declining line in the low-frequency region that corresponds to the diffusion-controlled process.[49,53] The R_{ct} values were calculated according to the equivalent circuit shown in the inset of Figure 7. Among the cells, the PCC5-based symmetrical cell showed an R_{ct} value of ~3.78 Ω, whereas R_{ct} values of ~10.99 and ~4.36 Ω are noted for PCC0 and PCC3, respectively. This result reveals the excellent conductivity of PCC5, which certainly provides the enhancement in the electrochemical profile especially at high current rates. In addition, the symmetric cell that comprises PCC5 exhibits a Warburg tail, which corroborates the excellent capacitive properties noted during both the potentiostatic and galvanostatic measurements.

As noted from the CV and galvanostatic studies, PCC5-based symmetric supercapacitors have favorable electrochemical properties. As a result, high energy and power densities are anticipated for such a supercapacitor assembly. Energy and power densities were calculated from the galvanostatic profiles (Figure S4) and are given in a Ragone plot (Figure 8). The deterioration of the energy density with the increasing power den-

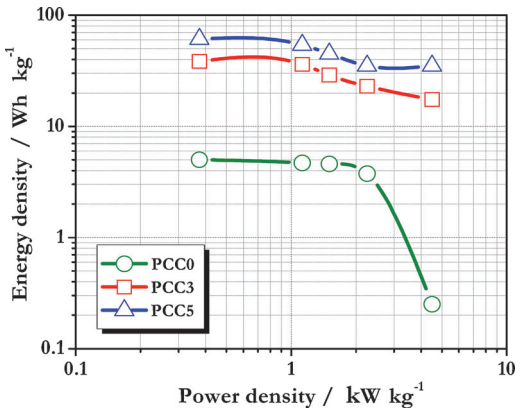

Figure 8. Ragone plots of PCC0-, PCC3-, and PCC5-based symmetric supercapacitor cells derived from Figure S3.

sity is because of the complex resistance and tortuous diffusion pathway within the porous textures. PCC5-based cells delivered the maximum energy density of ~61 Wh kg^{-1}, whereas PCC3- and PCC0-based cells presented energy densities of ~38 and ~5 Wh kg^{-1}, respectively. Notably, the energy density of the PCC5-based symmetrical cell is one of the best results obtained for EDLCs fabricated with other carbonaceous materials in nonaqueous media, such as AC fabric (~23 Wh kg^{-1}), carbon nanotubes (~49 Wh kg^{-1}), and other materials.[5,6,54–57] The superior electrochemical performance of pine-cone-derived AC is mainly a result of the following factors: (i) the high specific surface area (3950 m^2 g^{-1}) with a large pore volume (2.4 cm^3 g^{-1}) and microporosity, which provide a large number of reaction sites to result in the accumulation of charge carriers,[54] (ii) the excellent electrical conductivity and low charge-transfer resistance, which improves the kinetics significantly[2,7] and is favorable to overcome the kinetic limitations at high-current operation, (iii) the 3D architecture of the prepared AC provides structural integrity during prolonged cycling, (iv) the very low internal resistance offered by the cell (Figure S4), and (v) the presence of surface functional groups (Figure 3). These results suggest that the carbon derived from pine cones could be used as a high-performance electrode material for high-energy-density EDLC applications.

Conclusions

The great potential of the use of pine-cone-derived high-surface-area activated carbon in electrochemical double-layer capacitor applications was demonstrated in an organic medium with a high energy density in mind. The pyrolyzed carbon treated with 5 wt% KOH delivered favorable electrochemical properties in a symmetric supercapacitor configuration. The supercapacitor cell delivered the maximum energy density of ~61 Wh kg^{-1} with an excellent capacitance retention of ~90% after 20000 cycles. The results reported here provide a simple and effective way to prepare high-surface-area activated carbons from a low-cost, highly abundant biomass source, that is, pine cone petals. This could potentially facilitate the development of electrochemical double-layer capacitors with higher energy densities than the state-of-art activated carbon materials that are available commercially.

Experimental Section

Preparation of ACs

Mature female pine cone petals (Pinuscoulteri cone, PCC) were used as the starting material. The pine cone petals were washed with water and dried at 60 °C for 10 days. First, the pine cone petals were ground into a fine powder and treated with different weight ratios of KOH (1:0, 1:3, 1:5) at 110 °C for 5 h. Then, the mixture was pyrolyzed at 750 °C under an Ar flow at a heating rate of 5 °C min^{-1} for 1.5 h. After cooling to RT, the resultant product was washed thoroughly with 0.1 M HCl and deionized water several times to remove residual K^+ ions until the pH value of the washed solution was 6.5–7. The washed powder was vacuum dried and subsequently used for various characterization studies. PCC obtained with KOH weight ratios of 1:0, 1:3, and 1:5 are designated as PCC0, PCC3, and PCC5, respectively.

Physical characterization

Powder XRD patterns were recorded by using a Rigaku Rint 1000, Japan, using CuK_α as a radiation source. BET surface area measurements were performed by using a micromeritics ASAP 2010 surface area analyzer. Morphological features of the samples were recorded by using a scanning electron microscope (FE-SEM, S4700, Hitachi, Japan). Raman spectra of the prepared samples were recorded by using a Raman dispersive spectrometer (Lab Ram HR 800, Horiba, Japan). FTIR spectroscopy was performed by using an IR Presitge-21 spectrometer (Shimadzu, Japan).

Electrochemical characterization

All the electrochemical measurements were performed in a standard CR2032 coin-cell configuration. The composite electrodes were formulated with accurately weighed amounts of active material (5 mg; PCC0, PCC3, or PCC5), ketzen black (1 mg; KB), and Teflonized acetylene black (TAB-2; 1 mg) in ethanol. The slurry was pressed over a stainless-steel mesh (200 mm^2 area) and dried at 160 °C for 4 h in a vacuum oven. A symmetric supercapacitor assembly was constructed with two similar electrodes separated by a porous polypropylene (Celgard 3401, USA) film and filled with 1 M $LiPF_6$ in ethylene carbonate/dimethyl carbonate (1:1 v/v, Soulbrain Co. Ltd, Korea). CV and EIS studies were performed by using a Bio-Logic (SP-150), France, electrochemical work station. Galvanostatic charge–discharge studies were performed between 0–3 V at different current densities by using a conventional battery tester (WBCS 3000, Won-A-Tech, Korea) under ambient conditions. The electrochemical parameters such as specific capacitance, average internal resistance, coulombic efficiency, and energy and power densities of the supercapacitor were calculated by using formulas described elsewhere.[49,53,58,59]

Acknowledgements

This work was supported by the Energy Efficiency and Resources R&D program (20112010100150) under the Ministry of Knowledge Economy, Republic of Korea.

Keywords: biomass · carbon · electrochemistry · mesoporous materials · microporous materials

[1] N.-S. Choi, Z. Chen, S. A. Freunberger, X. Ji, Y.-K. Sun, K. Amine, G. Yushin, L. F. Nazar, J. Cho, P. G. Bruce, *Angew. Chem. Int. Ed.* **2012**, *51*, 9994 – 10024; *Angew. Chem.* **2012**, *124*, 10134 – 10166.
[2] P. Simon, P.-L. Taberna, F. Béguin in *Supercapacitors*, Wiley-VCH, Weinheim, **2013**, pp. 131 – 165.
[3] A. Burke, *Electrochim. Acta* **2007**, *53*, 1083 – 1091.
[4] E. Frackowiak, F. Béguin, *Carbon* **2001**, *39*, 937 – 950.
[5] D. S. Su, R. Schlögl, *ChemSusChem* **2010**, *3*, 136 – 168.
[6] M. Inagaki, H. Konno, O. Tanaike, *J. Power Sources* **2010**, *195*, 7880 – 7903.
[7] A. G. Pandolfo, A. F. Hollenkamp, *J. Power Sources* **2006**, *157*, 11 – 27.
[8] A. K. Shukla, T. Prem Kumar, *Curr. Sci.* **2008**, *94*, 314 – 331.
[9] T. Prem Kumar, T. Sri Devi Kumari, A. Manuel Stephan, *J. Indian Inst. Sci.* **2009**, *89*, 393 – 424.
[10] L. Wei, G. Yushin, *Nano Energy* **2012**, *1*, 552 – 565.
[11] M. Biswal, A. Banerjee, M. Deo, S. Ogale, *Energy Environ. Sci.* **2013**, *6*, 1249 – 1259.
[12] L. Wei, M. Sevilla, A. B. Fuertes, R. Mokaya, G. Yushin, *Adv. Energy Mater.* **2011**, *1*, 356 – 361.
[13] L. Wei, M. Sevilla, A. B. Fuertes, R. Mokaya, G. Yushin, *Adv. Funct. Mater.* **2012**, *22*, 827 – 834.
[14] M. S. Dandekar, G. Arabale, K. Vijayamohanan, *J. Power Sources* **2005**, *141*, 198 – 203.
[15] F.-C. Wu, R.-L. Tseng, C.-C. Hu, C.-C. Wang, *J. Power Sources* **2004**, *138*, 351 – 359.
[16] F.-C. Wu, R.-L. Tseng, C.-C. Hu, C.-C. Wang, *J. Power Sources* **2005**, *144*, 302 – 309.
[17] Y.-J. Kim, B.-J. Lee, H. Suezaki, T. Chino, Y. Abe, T. Yanagiura, K. C. Park, M. Endo, *Carbon* **2006**, *44*, 1592 – 1595.
[18] V. Subramanian, C. Luo, A. M. Stephan, K. S. Nahm, S. Thomas, B. Wei, *J. Phys. Chem. C* **2007**, *111*, 7527 – 7531.
[19] M. S. Balathanigaimani, W.-G. Shim, M.-J. Lee, C. Kim, J.-W. Lee, H. Moon, *Electrochem. Commun.* **2008**, *10*, 868 – 871.
[20] T. E. Rufford, D. Hulicova-Jurcakova, K. Khosla, Z. Zhu, G. Q. Lu, *J. Power Sources* **2010**, *195*, 912 – 918.
[21] B. Xu, Y. Chen, G. Wei, G. Cao, H. Zhang, Y. Yang, *Mater. Chem. Phys.* **2010**, *124*, 504 – 509.
[22] X. Li, W. Xing, S. Zhuo, J. Zhou, F. Li, S.-Z. Qiao, G.-Q. Lu, *Bioresour. Technol.* **2011**, *102*, 1118 – 1123.
[23] T. E. Rufford, D. Hulicova-Jurcakova, E. Fiset, Z. Zhu, G. Q. Lu, *Electrochem. Commun.* **2009**, *11*, 974 – 977.
[24] M. R. Jisha, Y. J. Hwang, J. S. Shin, K. S. Nahm, T. Prem Kumar, K. Karthikeyan, N. Dhanikaivelu, D. Kalpana, N. G. Renganathan, A. M. Stephan, *Mater. Chem. Phys.* **2009**, *115*, 33 – 39.
[25] X. Li, C. Han, X. Chen, C. Shi, *Microporous Mesoporous Mater.* **2010**, *131*, 303 – 309.
[26] W. Chen, H. Zhang, Y. Huang, W. Wang, *J. Mater. Chem.* **2010**, *20*, 4773 – 4775.
[27] Z. Li, L. Zhang, B. S. Amirkhiz, X. Tan, Z. Xu, H. Wang, B. C. Olsen, C. M. B. Holt, D. Mitlin, *Adv. Energy Mater.* **2012**, *2*, 431 – 437.
[28] M. Olivares-Marín, J. A. Fernández, M. J. Lázaro, C. Fernández-González, A. Macías-García, V. Gómez-Serrano, F. Stoeckli, T. A. Centeno, *Mater. Chem. Phys.* **2009**, *114*, 323 – 327.
[29] Y. Guo, J. Qi, Y. Jiang, S. Yang, Z. Wang, H. Xu, *Mater. Chem. Phys.* **2003**, *80*, 704 – 709.
[30] D. Kalpana, S. H. Cho, S. B. Lee, Y. S. Lee, R. Misra, N. G. Renganathan, *J. Power Sources* **2009**, *190*, 587 – 591.
[31] A. E. Ismanto, S. Wang, F. E. Soetaredjo, S. Ismadji, *Bioresour. Technol.* **2010**, *101*, 3534 – 3540.
[32] A. Elmouwahidi, Z. Zapata-Benabithe, F. Carrasco-Marín, C. Moreno-Castilla, *Bioresour. Technol.* **2012**, *111*, 185 – 190.
[33] M. P. Bichat, E. Raymundo-Piñero, F. Béguin, *Carbon* **2010**, *48*, 4351 – 4361.
[34] H. Haykırı-Açma, *Energy Convers. Manage.* **2003**, *44*, 155 – 162.
[35] G. Duman, Y. Onal, C. Okutucu, S. Onenc, J. Yanik, *Energy Fuels* **2009**, *23*, 2197 – 2204.
[36] M. Momčilović, M. Purenović, A. Bojić, A. Zarubica, M. Ranđelović, *Desalination* **2011**, *276*, 53 – 59.
[37] M. Hadi, M. R. Samarghandi, G. McKay, *Chem. Eng. J.* **2010**, *160*, 408 – 416.
[38] N. M. Mahmoodi, B. Hayati, M. Arami, C. Lan, *Desalination* **2011**, *268*, 117 – 125.
[39] M. Hadi, M. Samarghandi, G. McKay, *Water Air Soil Pollut.* **2011**, *218*, 197 – 212.
[40] P. Simon, Y. Gogotsi, *Nat. Mater.* **2008**, *7*, 845 – 854.
[41] E. B. Naidoo, A. Pholosi, A. E. Ofomaja, *Pure Appl. Chem.* **2013**, *85*, 2209 – 2215.
[42] A. E. Ofomaja, E. B. Naidoo, *Chem. Eng. J.* **2011**, *175*, 260 – 270.
[43] F. Z. Arrakhiz, M. El Achaby, K. Benmoussa, R. Bouhfid, E. M. Essassi, A. Qaiss, *Mater. Des.* **2012**, *40*, 528 – 535.
[44] Y. Liu, J. S. Xue, T. Zheng, J. R. Dahn, *Carbon* **1996**, *34*, 193 – 200.
[45] P. Suresh Kumar, R. Sahay, V. Aravindan, J. Sundaramurthy, W. C. Ling, V. Thavasi, S. Mhaisalkar, S. Madhavi, S. Ramakrishna, *J. Phys. D* **2012**, *45*, 265302.
[46] D.-W. Wang, A. Du, E. Taran, G. Q. Lu, I. R. Gentle, *J. Mater. Chem.* **2012**, *22*, 21085 – 21091.
[47] N. Kumar, R. Radhika, A. T. Kozakov, K. J. Sankaran, S. Dash, A. K. Tyagi, N. H. Tai, I. N. Lin, *J. Phys. D* **2013**, *46*, 275501.
[48] H.-J. Oh, J.-H. Lee, H.-J. Ahn, Y. Jeong, Y.-J. Kim, C.-S. Chi, *Thin Solid Films* **2006**, *515*, 220 – 225.
[49] K. Karthikeyan, S. Amaresh, V. Aravindan, H. Kim, K. S. Kang, Y. S. Lee, *J. Mater. Chem. A* **2013**, *1*, 707 – 714.
[50] Y. Korenblit, M. Rose, E. Kockrick, L. Borchardt, A. Kvit, S. Kaskel, G. Yushin, *ACS Nano* **2010**, *4*, 1337 – 1344.
[51] J. Chmiola, G. Yushin, Y. Gogotsi, C. Portet, P. Simon, P. L. Taberna, *Science* **2006**, *313*, 1760 – 1763.
[52] A. Jain, V. Aravindan, S. Jayaraman, P. S. Kumar, R. Balasubramanian, S. Ramakrishna, S. Madhavi, M. Srinivasan, *Sci. Rep.* **2013**, *3*, 3002.
[53] K. Karthikeyan, S. Amaresh, V. Aravindan, Y. S. Lee, *J. Mater. Chem. A* **2013**, *1*, 4105 – 4111.
[54] M. Seredych, D. Hulicova-Jurcakova, G. Q. Lu, T. J. Bandosz, *Carbon* **2008**, *46*, 1475 – 1488.
[55] E. Frackowiak, *Phys. Chem. Chem. Phys.* **2007**, *9*, 1774 – 1785.
[56] J. Wang, S. Kaskel, *J. Mater. Chem.* **2012**, *22*, 23710 – 23725.
[57] G. Gryglewicz, J. Machnikowski, E. Lorenc-Grabowska, G. Lota, E. Frackowiak, *Electrochim. Acta* **2005**, *50*, 1197 – 1206.
[58] Y. Zhu, S. Murali, M. D. Stoller, K. J. Ganesh, W. Cai, P. J. Ferreira, A. Pirkle, R. M. Wallace, K. A. Cychosz, M. Thommes, D. Su, E. A. Stach, R. S. Ruoff, *Science* **2011**, *332*, 1537 – 1541.
[59] M. D. Stoller, R. S. Ruoff, *Energy Environ. Sci.* **2010**, *3*, 1294 – 1301.

Received: November 24, 2013
Revised: January 18, 2014
Published online on March 19, 2014